Analysis of entropy and effect of surface dynamics on photovoltaic performance

Analysis of entropy and effect of surface dynamics on photovoltaic performance

[1]**Abodunrin T.J.**, [1]**Usikalu M.R.**, [1]**Emetere M.E.**, [2]**Yenus Z.**, [2]**Kotsedi C.**, [2]**Maaza M.**

[1]Department of Physics, Covenant University, P.M.B. 1023, Ota, Ogun State, Nigeria.
[2]iThemba Labs, P.O Box 722, Somerset West 7129, Western Cape, South Africa.

temitope.abodunrin@covenantuniversity.edu.ng

Abstract.
We investigate the influences of photoanode on light scattering and absorption in a dye-sensitized solar cell (DSSC). N719 dye on a monolayer anode of TiO_2 film and ZnO film, are compared in terms of their photovoltaic conversion efficiency. Doctor blade application and high temperature sintering of photoanode assemblage on indium doped tin oxide glass was adopted for preparation of the two photoanodes. The optical density of the interfacial layer relative to the photogenerated carriers is determined by absorption of ionic electrolytes. The outcome obtained with different photosensitizing effect of organic *T.daniellii*molecules on DSSCs showed a wide disparity, the highest V_{oc} was recorded with Br^- with 500 mV and 79 mV respectively for TiO_2 and ZnO photoanode respectively. Three important morphological characterization techniques were used, scanning electron microscopy (SEM) with energy dispersive spectrum (EDS), Electron shell occupancy and Entropy were discussed in detail with respect to their photoelectric performance, the best $I_{sc}$was 0.035 mA with Br^- on TiO_2 attributable to a large optical density, achieved from ratio of area of molecular coverage of nanoparticle film. Scanning electron microscopy (SEM) revealed a structure consisting of direct and ordered paths for photogenerated carriers to the collecting electrodes, the P_{max}result reported was 36.54 mW with Br^- from TiO_2.

1. Introduction

Inauguration of DSSCs technology by O'Regan and Grätzel ushered generation of clean sources of energy directly from the enormous power of the Sun [1]. In spite of their relatively low efficiency compared to perovskites, they are still regarded as prospective energy sources owing to their low manufacturing cost, ability to operate under conditions

of poor lighting and ease of disposal [2-5]. Even though many semiconductor oxides such as ZnO, $Fe2O_3$, SnO_2, NiO_2, TiO_2 have been examined for efficient light-to-electric conversion prospects in DSSCs. Structural and material engineering of DSSCs still present a prototype for the interrelationship between charge-transfer dynamics and efficiency record [6]. Succession of organic dyes with donor−π-linker–acceptor (D−π–A) framework has been employed as candidates for competent intramolecular charge separation [7]. Tailoring the design strategy by varying the conjugation length of the linker unit has been observed to influence an enlargement in spectral absorption of the sensitizer thereby, which boosts the photocurrent generation [8]. Photovoltaic performance of DSSC is categorized by electrochemical and photophysical analysis, function of charge recombination and dye regeneration dynamics using transient absorption spectroscopic measurements [9]. Kinetics of charge transfer after electron injection to dye/semiconductor interface within femtosecond to millisecond, simultaneous photon absorption by dye sensitizers, intramolecular charge separation within the conduction band of the semiconductor [10]. Thus, it is crucial to obtain a balance in the engineering of the dye/photoanode interface and electron injection/recombination dynamics in order to successfully monitor the microscopic events that govern interfacial results andcharacterization in DSSCs [11]. This research seeks to design mesoporous crystalline TiO2 and ZnO for efficient utilization of the solar spectrum and enhancement of photovoltaic conversion efficiency (η), and consequently determine the most convincing material for DSSC photoanodes.

2. Methodology

Two groups of Solar cells with active area of 3.16 cm_2 were assembled. The first group comprising of three solar cells was deposited with TiO_2 colloidal suspension using the doctor blading method of application onto indium doped tin oxide (ITO). A second set comprising of three solar cells unit was masked with ZnO suspension. The colloidal paste was prepared from 20 g mass of dry powder form of TiO_2 and ZnO Degussa of commercial variety respectively, dissolved in conc. 1M HNO_3 and stirred continuously for 0.5 h. Two drops of ethanol were added to each of the mixture in order to boost the cohesivity of the colloids. Each of the photoanode film was further subjected to high temperature sintering at 450 ◦C for 1.5 h in a simulated autoclave, after which they were brought out to cool. On assuming room temperature, they were replaced in the autoclave for re-heating but this time only for 0.5 h. *T.daniellii*dye comprising of 1 g dye: 100ml of 1M Ethanol, was soaked into each of the photoanode thin film surface when the setup assumed room temperature. The counter electrodes were prepared by exposing the conducting slides to a naked Bunsen flame and depositing trilayer of soot in a simulated vacuum. After 24 h, the counter electrode was pressed onto the top of the TiO_2/ITO and ZnO/ITO photoanode films using binder clips. 1 ml of aqueous of electrolytic solutions of potassium iodide, bromide and chloride were used to sensitize each unit of DSSC. The DSSC samples were connected in parallel with a variable load and digital multimeter and exposed under standard conditions of 1 atmosphere [12]. Scanning electron microscopy of *T.daniellii* on different electrodes was carried out to understand the molecular interaction. Energy dispersive spectrum revealed the elemental composition for different photoanodes and software interpretation with Gwydion exposed a novel facet on interrelationship of electron occupancy with photocurrent generation and the entropy.

3. Results and Discussion

3.1. *SEM with Energy Dispersive Spectrum Microscopy*

T.daniellii microstructural details in high resolution image at 25 μm and elemental composition and identification is presented in Figure 1(a), (b) and (c) with KCl, KBr and KI electrolytes respectively. Illustration of the quantitative composition is given in Table 1. The proportions contrast in accordance with the alignment of *T.daniellii* individual particle relative to the entire specimen surface and gradient. A higher number of *T.daniellii* nanocomposites has above 50% composition of C and O, an allusion to the organic of the dye with an exception of *T.daniellii* + ZnO + KBr. The second largest proportion of the element is from the photoanode material, this factor is constant for all four microstructures considered.

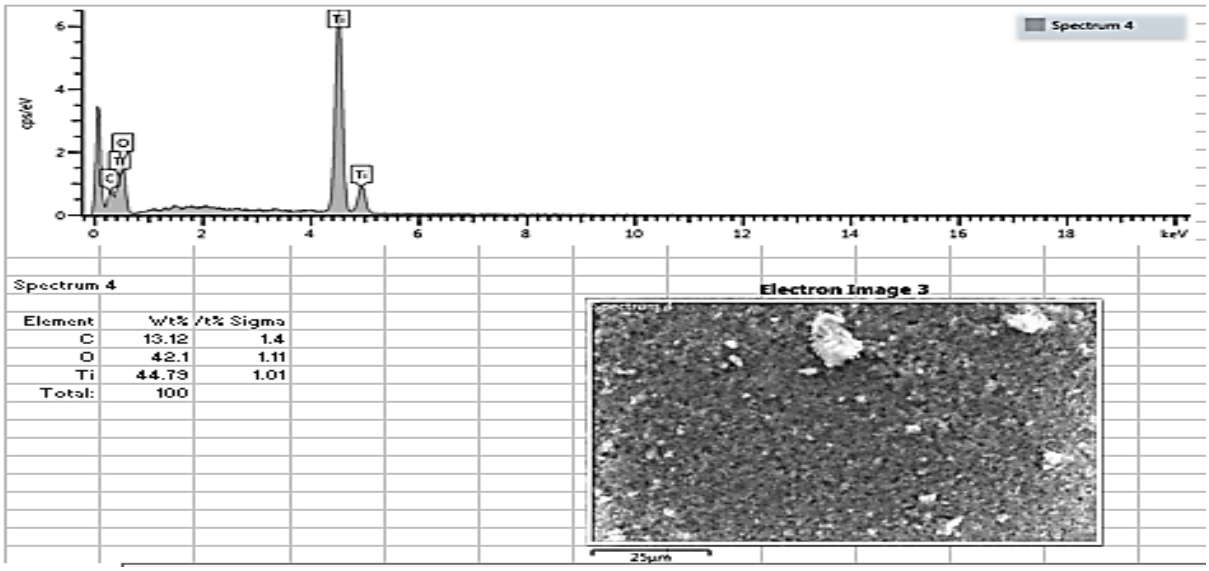

Figure 1(a): *T.daniellii* +TiO_2+KCl

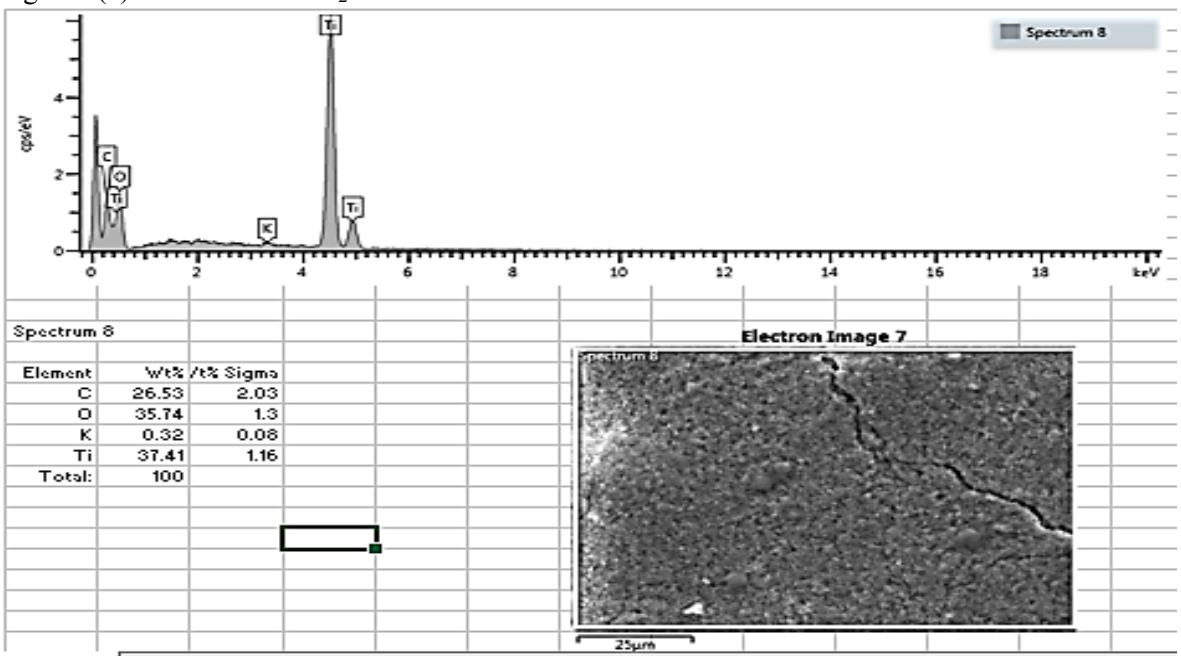

Figure 1(b): *T.daniellii* +TiO_2+KBr

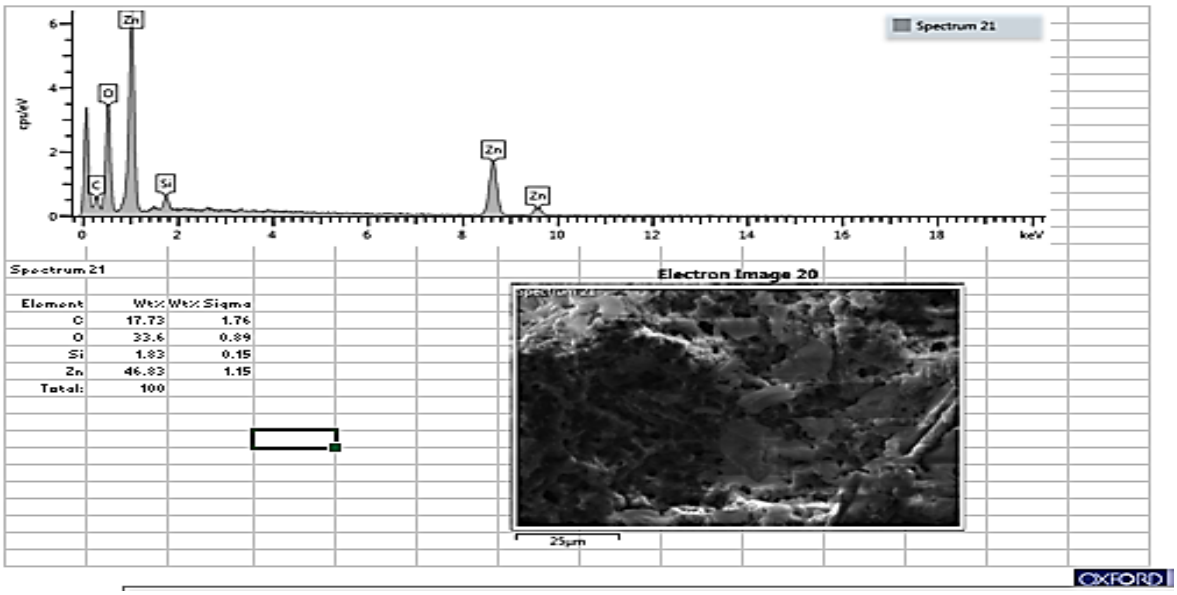

Figure 1(c): *T.daniellii* + ZnO + KI

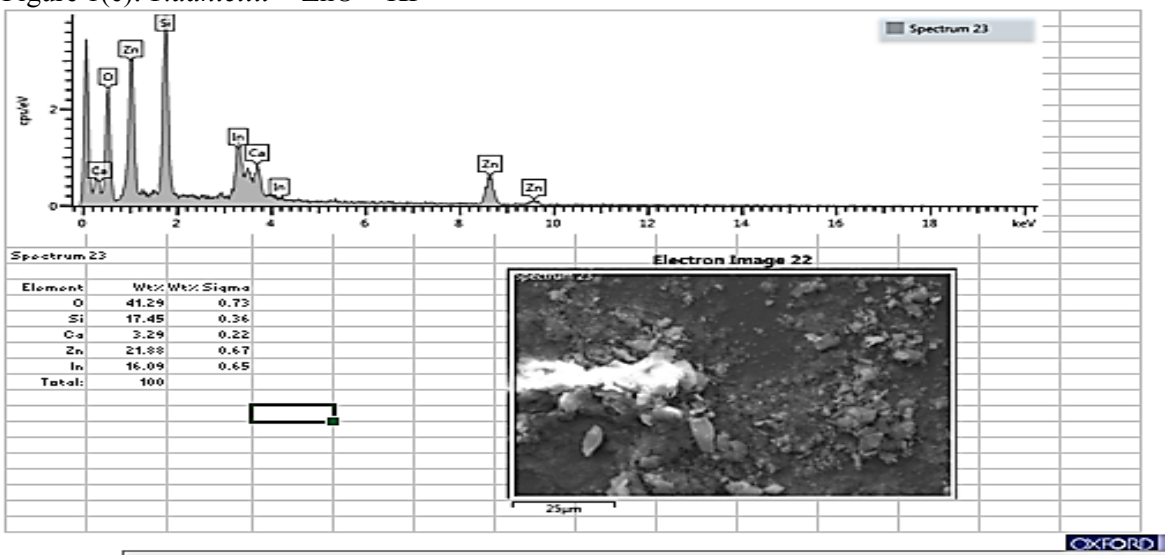

Figure 1(d): *T.daniellii* + ZnO + KBr

Table 1: Analysis of SEM with EDS spectroscopy of *T.daniellii* on different photoanodes

	DSSC Composition	C-O (%)	Photoanode (%)
1.	*T.daniellii* +TiO_2+KCl	55.22	44.79
2.	*T.daniellii* +TiO_2+KBr	62.27	37.41
3.	*T.daniellii* + ZnO + KI	51.33	46.83
4.	*T.daniellii* + ZnO + KBr	41.29 (Oxygen only)	21.88

Note: Highlight shows the highest photoanode composition

3.2. *Electron shell occupancy spectroscopy*

Gwydion program software was used to obtain the way the electrons would hop in *T.daniellii* microstructure. The red dots signify electron seats which represent the highest probability of occupancy as electrons diffuse by hopping along the cross-sectional area. Blue region shows the regions with a high rate of electron tunnelling where recombination is most likely to occur. In Figure 2

(a), the midsection of electron seats is cut off from the peripheral section by the blue tunnelling zone. Electron tunnelling will be very pronounced in this situation and similarly in 2 (d) [13-14].

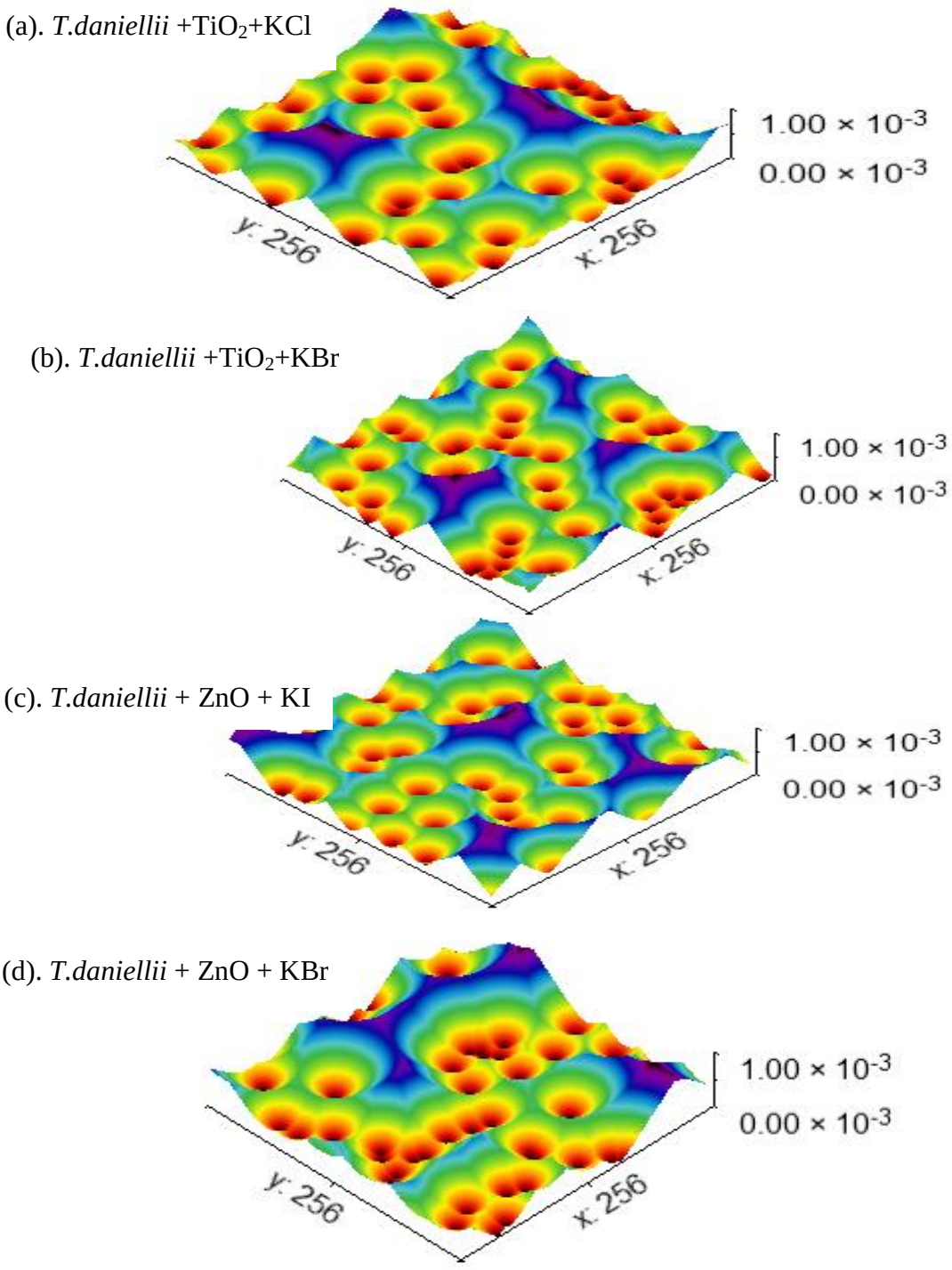

Figure 2: Schematic Representation of Electron Occupancy in *T.daniellii*

3.3. Entropy (S) Measurement in T.daniellii DSSCs

The number of configurations *T.daniellii* can exist increases under illumination, the charge transport will be along the path of least resistance. This will preferably be in solution rather than in the

photoanode framework. Thus, only the dyes affixed onto the photoanode frame are part of the conduit of charge flow under illumination. Electrons close to the fringes or peripheral are liable to recombine before arrival on the photoanode framework . A non -negative S is used to express the effect of excitation of *T.daniellii* dye molecules which ought to be greater than the entropy of the source of illumination [13]. Consequently, *T.daniellii*/TiO_2/KBr photoanode records a negative value of entropy, the entropy of illuminating source is larger than its intrinsic entropy after excitation. The highest entropy is revealed in *T.daniellii*/ZnO/KI as shown on Table 2 and illustrated graphically by Figure 3 (a) to (d). However, the entropy deficit of *T.daniellii*/TiO_2/KBr is much lesser than *T.daniellii*/TiO_2/KCl. This parameter refers to the measure of inhomogeneity as shown in Equation 1. *T.daniellii*/ZnO/KI has a deficit very minimal relative to *T.daniellii*/ZnO/KBr on ZnO photoanode. The least entropy value was recorded in *T.daniellii*/ZnO/KBr. An inverse relationship exists between Entropy and photocurrent generation as shown on Table 3.

Table 2: Entropy of *T.daniellii* Photoanodes

	Entropy ($J \cdot K^{-1}$)	Entropy deficit	Photoanode
1.	5.06469	0.481345	*T.daniellii*/TiO_2/KCl
2.	-7.18081	0.0452494	*T.daniellii*/TiO_2/KBr
3.	5.18333	0.258918	*T.daniellii*/ZnO/KI
4.	4.3557	1.19956	*T.daniellii*/ZnO/KBr

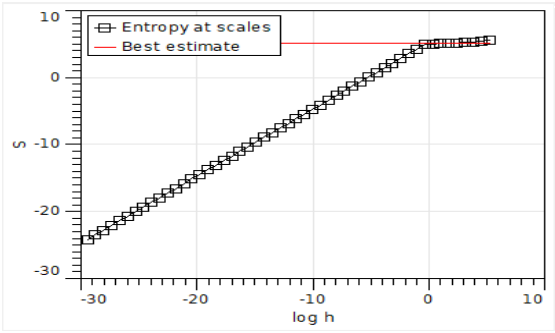

(a) *T.daniellii* +TiO_2+KCl

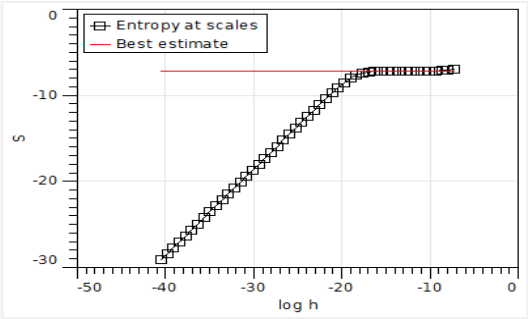

(b). *T.daniellii* +TiO_2+KBr

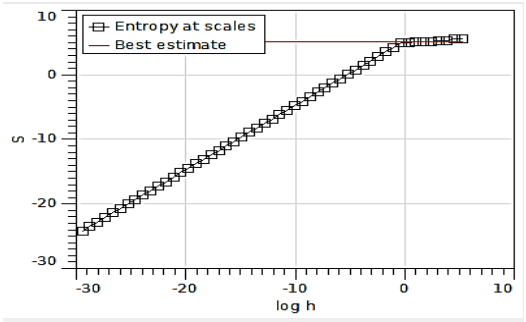

(c). *T.daniellii* + ZnO + KI

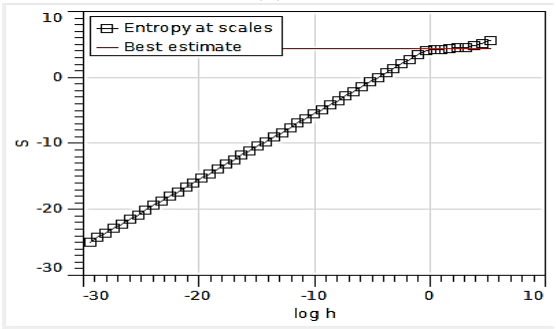

(d). *T.daniellii* + ZnO + KBr

Figure 3: Graphical illustration of entropy of *T.daniellii* nanocomposites

Table 3: Photo current generation of *T.daniellii* DSSCs

	TiO_2 Photoanode			ZnO Photoanode		
Electrolyte	I_{sc} (mA)	V_{oc} (mV)	P_{max} (mW)	I_{sc} (mA)	V_{oc} (mV)	P_{max} (mW)
KCl	1.45×10^{-4}	0.57	4.90×10^{-7}	0.003	18.0	0.060
KI	2.5×10^{-4}	4.30	1.56×10^{-3}	0.013	16.3	0.163
KBr	3.5×10^{-2}	590	36.54	0.023	79.0	1.728

$$S_{max} - S_{actual} = Entropy\ deficit \quad (1)$$

3.4. Photoelectric Performance of T.daniellii DSSCs on Different Photoanodes

The comparative output performance of *T.daniellii* dye based on different Photoanode materials is as shown in Figure 4 (a) - (f). The best I_{sc}, V_{oc} and P_{max} was recorded in KBr/TiO_2 and the least I_{sc} ,V_{oc} and P_{max} was observed in KCl/TiO_2, this corroborates the highest $I_{sc,}V_{oc}$ and P_{max} in KBr/ZnO. Thus, TiO_2 photoanode shows above 50% efficiency compared to ZnO photoanode for V_{oc} in KBr as shown in Figure 5 (a) and (b). This is consequent of the factor of ZnO forming soluble aggregates with substances when it is involved in any chemical reaction. In effect, this promotes agglutination, recombination and hysteresis loss in DSSCs. In ZnO, KBr produced the least whereas KI recorded the best output which is a direct consequence of the entropy of the reaction but different from the photocurrent generation in Table 3. In TiO_2 photoanode, KBr had less entropy deficit than KCl, this accounts for the better output for KBr. This implies that the entropy deficit for KI, would be even lesser than that of KBr by implication.

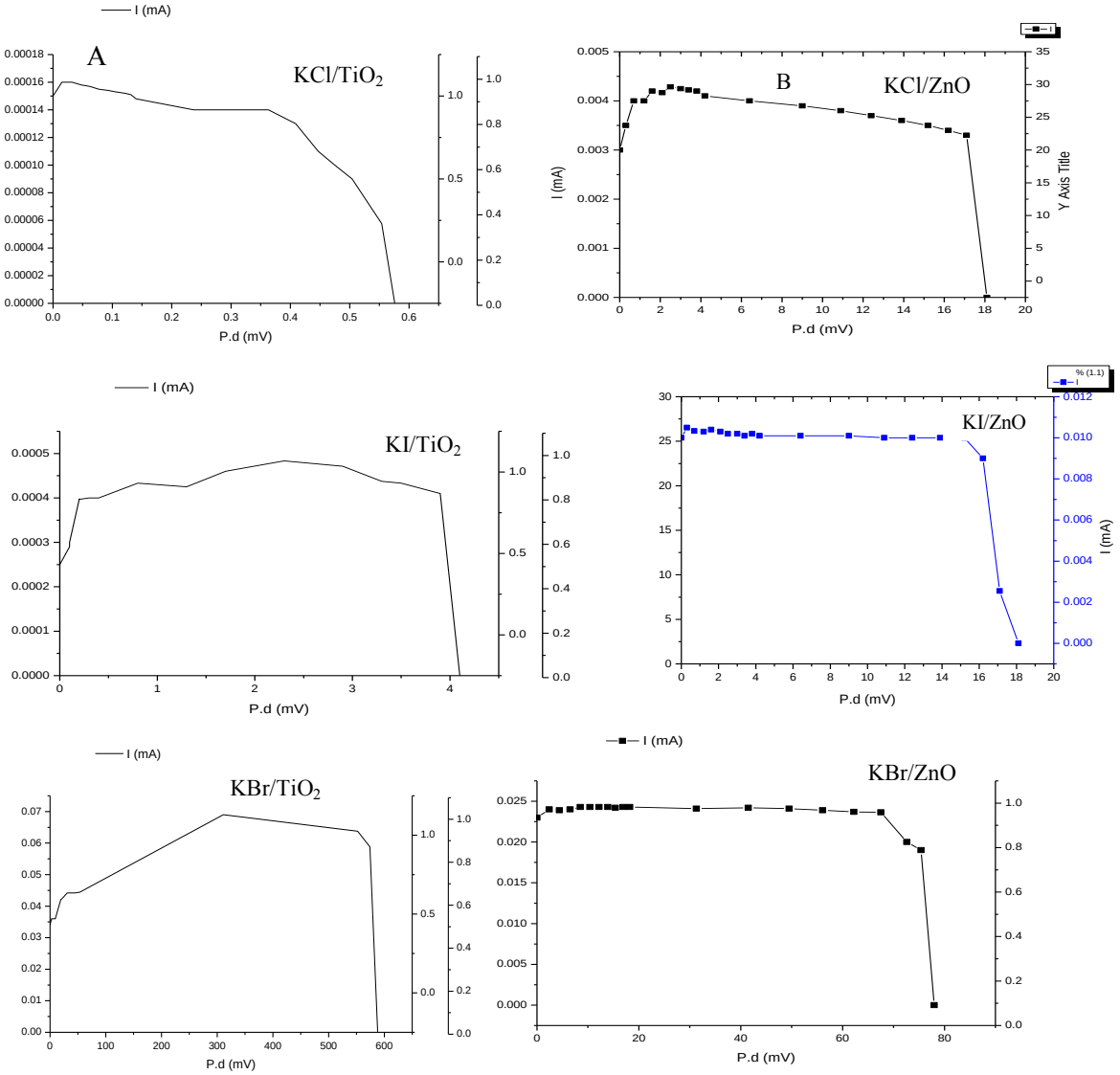

Figure 4: I-V Characteristics of *T.daniellii*DSSCs with electrolytic ions on different electrodes

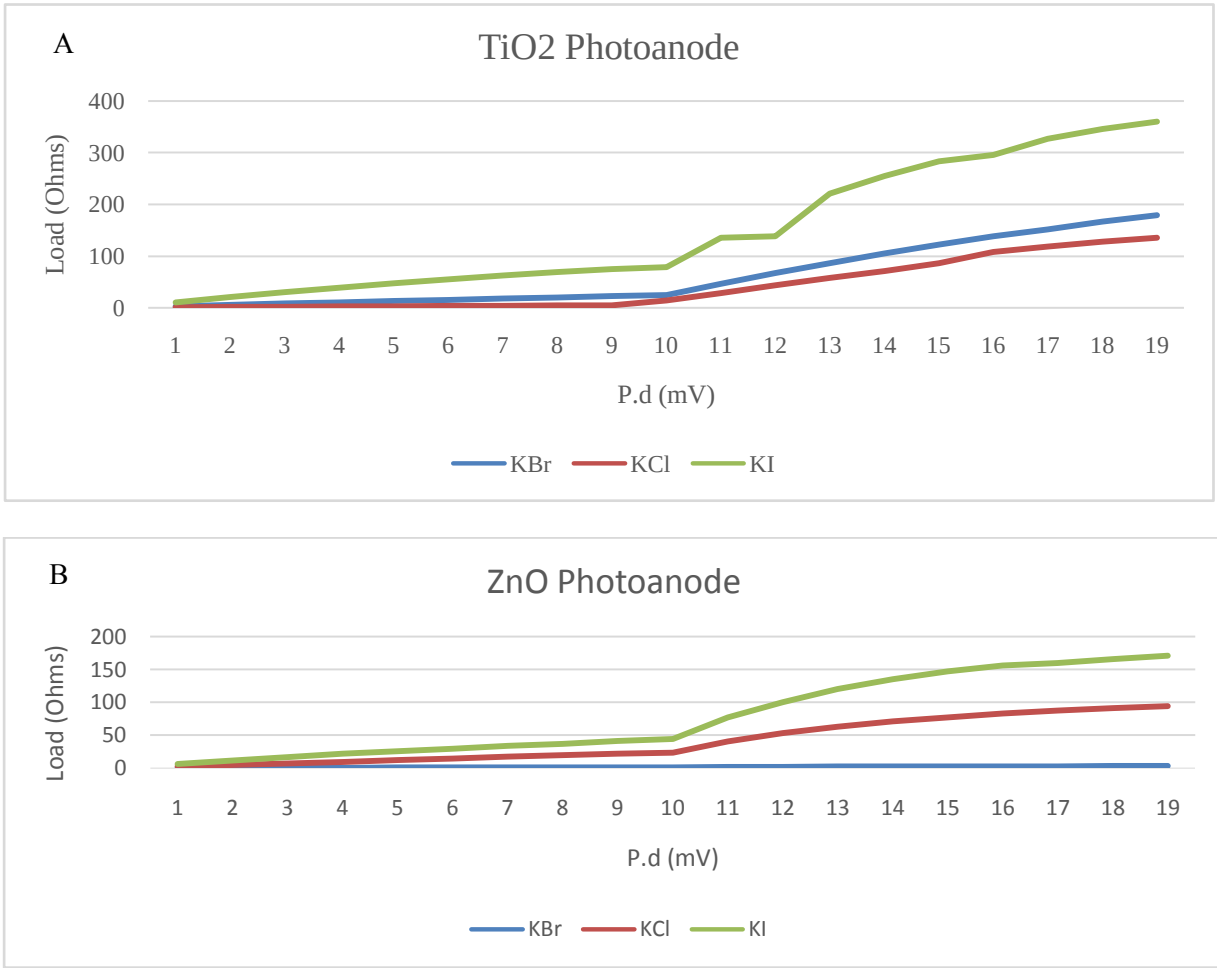

Figure 5: Measurement of *T.daniellii* Photoelectric Performance on different photoanodes

Conclusion and Recommendation

Our study reveals the following results:

1. Bromide (Br^-) ions favor the $TiO_2$and ZnOphotoanode, it promotes the forward kinematics of *T.daniellii* DSSCs due to their less activation potential. Thus, electron charge carriers on these interfaces successfully migrate due to better interstitial kinematics as the iodide articulates with the photoanode surfaces.
2. Cl^- and I^-charge transport is enhanced on ZnO photoanode but impeded on TiO_2.
3. Entropy calculations for KBr/TiO_2 and KBr/ZnOhave the least values. This is an indication that, entropy is inversely proportional to photoelectric performance, when all other conditions remain constant.
4. However, the preferred electrode is TiO_2 as indicated by the maximum power value, about 7.5 times higher than that observed for ZnO.

Bilayer application of iodide on the dual combination of TiO_2 and ZnO is encouraged for possible enhancement of photovoltaic output in future research applications.

Acknowledgement

The authors wish to express their profound gratitude to Covenant University and iThemba laboratories for providing a suitable environment for the successful completion of this work.

References

[1] S. Agarwala, M. Kevin, A.S.W. Wong, C.K.N. Peh, V. Thavasi, G.W. Ho.(2010). Mesophase Ordering of TiO_2 Film with High Surface Area and Strong Light Harvesting for Dye-Sensitized Solar Cell. *ACSAppl. Mater. Interfaces*, 2, 1844-1850.

[2] C. Prasittichai, J. T. Hupp. (2010). Surface modification of SnO_2 photoelectrodes in dye-sensitized solar cells: significant improvements in photovoltage via Al_2O_3 atomic layer deposition. *J. Phys Chem Lett*, 1, 1611-1615.

[3] I.T. Choi, M.J. Ju, S.H. Song, S.G. Kim, D.W. Cho, C. Im, H.K. Kim. Chem. Eur. J., (2013). Synthesis and optical nonlinear properties of novel Y-shaped chromophores with excellent electro-optic activity. *Journal of Material Chemistry*, 23, 15545-15555.

[4] A. Sedghi, H.N. Miankushki. Influence of $TiCl_4$ treatment on structure and performance of dye-sensitized solar cells. *Jpn J Appl Phys*, 52 (2013), 075002.

[5] W.E. Ghann, H. Kang, J. Uddin, F. Chowdhury, S.I. AKhondaker, M. Moniruzzaman, M.H. Kabir,M.M. Rahman (2019). Synthesis and characterization of reduced graphene oxide and their application in dye-sensitized solar cell. *Chem. Eng.*, 3 (1) 7.

[6] D. Wang, S. Liu, M. Shao, J. Zhao, Y. Gu, Q. Li, X. Zhang, J. Zhao, Y. Fang (2018). Design of SnO_2 aggregate/nanosheet composite structures based on functionmatching strategy for enhanced dye-sensitized solar cell performance. *Mater*, 11 (9) 1774.

[7] G.R.A. Kumara, U. Deshapriya, C.S.K. Ranasinghe, E.N. Jayaweera, R.M.G. Rajapakse (2018). Efficient dye-sensitized solar cell from mesoporous zinc oxide nanostructures sensitized by N719 dye. *J. Semicond*, 39 (3) 033005.

[8] L. Yan, F.L. Wu, L. Peng, L.J. Zhang, P.J. Li, S.Y. Dou, T.X. Li (2012). Photoanode of dye-sensitized solar cell based on a ZnO/TiO_2 composite film. *Int. J. Photoenerg*. Article ID 613969.

[9] X. Liu, J. Fang, Y. Liu. T. Lin (2016). Progress in nanostructured photoanodes for dye-sensitized solar cell. *Front. Mater. Sci.* 10 (3), 225-237.

[10] S.-W. Lee, K.-S. Ahn, K. Zhu, N.R. Neale, A.J. Frank (2012). Effects of $TiCl_4$ treatment of nanoporous TiO_2 films on morphology, light harvesting, and charge-carrier dynamics in dye-sensitized solar cells. *J. Phys Chem C*, 116, 21285-21290.

[11] N.G. Park, J. Van De Lagemaat, A.J. Frank (2000). Comparison of dye-sensitized rutile-and anatase based TiO_2solar cell. *J. Phys. Chem. B* 104 (38), 8989-8994.

[12] T.J. Abodunrin, A.O. Boyo, M.R. Usikalu (2018). Data on the porphyrin effect and influence of dopant ions on *Thaumatococcus daniellii* dye as sensitizer in dye-sensitized solar cells. *Data in* Brief, 20, 2020-2026.

[13] T.J. Abodunrin, A.O. Boyo,M.R. Usikalu, L.N. Obafemi,O.F. Oladapo (2017). Theprospect of micro-energy generation from almond (*Prunus dulcis*) dye-sensitized solar cells. *Journal of Infomatics and Mathematical Sciences* 9 (2), 231-239.

[14] T.J. Abodunrin, A.O. Boyo, M.R. Usikalu, O. Kensinro (2018). Spectral responses of B.vulgaris dye-sensitized solar cells to change in electrolyte. *IOP Conference Series: Earth and Environmental Science* 173 (1), 012047.

[15] T. J. Abodunrin, M. E. Emetere, O. O. Ajayi, U. O. Uyor, O. Popoola (2019). Investigating the prospect of micro-energy generation in S. Anisatum Dye-sensitized solar cells (DSCs). Journal of Physics: Conference Series 1299 (1), 012028.